JOURNAL OF GEOPHYSICAL RESEARCH, VOL. 100, NO. A9, PAGES 17,117–17,128, SEPTEMBER 1, 1995

Damping and spectral formation of upstream whistlers

D. S. Orlowski and C. T. Russell

Institute of Geophysics and Planetary Physics, University of California, Los Angeles

D. Krauss-Varban and N. Omidi

Department of Electrical and Computer Engineering and California Space Institute, University of California San Diego, La Jolla

M. F. Thomsen

Los Alamos National Laboratory, Los Alamos, New Mexico

Abstract. Previous studies have indicated that damping rates of upstream whistlers strongly depend on the details of the electron distribution function. Moreover, detailed analysis of Doppler shift and the whistler dispersion relation indicate that upstream whistlers propagate obliquely in a finite band of frequencies. In this paper we present results of a kinetic calculation of damping lengths of wideband whistlers using the sum of seven drifting bi-Maxwellian electron distributions as a best fit to the ISEE 1 electron data. For two cases, when upstream whistlers are observed, convective damping lengths derived from ISEE magnetic field and ephemeris data are compared with theoretical results. We find that the calculated convective damping lengths are consistent with the data and that upstream whistlers remain marginally stable. We also show that the slope of plasma frame spectra of upstream whistlers, obtained by direct fitting of the observed spectra, is between 5 and 7. The overall spectral, wave, and particle characteristics, proximity to the shock, as well as propagation and damping properties indicate that these waves cannot be generated locally. Instead, the observed upstream whistlers arise in the shock ramp, most likely by a variety of cross-field drift and/or anisotropy driven instabilities.

1. Introduction

The discovery by OGO 5 of electromagnetic waves with frequencies between 0.5 and 4 Hz in the unshocked solar wind, magnetically connected to the Earth's bow shock [*Russell et al.*, 1971], provided some of the first evidence of significant local processes associated with collisionless shocks not predicted by (ideal) MHD theory [*Holzer et al.*, 1972]. Statistical analysis and detailed calculations [*Fairfield*, 1974], based on the cold plasma approximation [*Stix*, 1962] using power spectral analysis methods [*Arthur et al.*, 1976], indicated that these waves propagate obliquely in the whistler mode. Moreover, the Doppler shift effect was found to strongly affect spacecraft frame polarizations and spectral density. While in the literature these waves were generally called the One Hertz waves, [*Hoppe et al.*, 1982, and references therein] the later discovery of similar waves in the Venus, Mercury, and Saturn foreshocks [*Orlowski et al.* 1990,1992; *Orlowski and Russell*, 1991] at substantially different frequencies prompted us to refer to these waves as upstream whistlers [*Orlowski et al.* 1993]. *Fairfield* [1974] hypothesized that the shock was the source of these waves. However he did not propose a precise mechanism for the generation of these waves by the shock. He also did not address the crucial question of the apparently nearly undamped propagation necessary for these waves to be observed so far from the shock. Moreover, later studies [*Rodriguez and Gurnett*, 1975, *Greenstadt et al.*, 1981] indicated that the shock-generated whistlers are subject of heavy damping in the shock foot and are unlikely to reach the deep foreshock.

These unsolved problems prompted other authors to explore alternate mechanisms for the generation of upstream waves, especially when the ISEE 1 and 2 high-resolution particle measurements revealed a wide variety of nonthermal proton and electron populations in the Earth's foreshock [*Paschmann et al.*, 1981]. A detailed mechanism for their generation by anisotropic or gyrophase bunched proton beams was developed by *Wong and Goldstein*, [1987, 1988]. However, this mechanism was not able to explain the bulk of the observations when neither anisotropy nor phase bunching was evident in the data [*Hoppe et al.*, 1982]. Therefore we do not discuss this hypothesis, further here. Another local generation hypothesis was *Sentman et al.*'s [1983] and was motivated by apparent correspondence between upstream whistler observations and the presence of suprathermal, large pitch angle electrons backstreaming from the shock [*Feldman et al.*, 1983]. With the publication of this work the hypothesis of *Fairfield* [1974] was generally forgotten. However, not all the properties of the waves were predicted by the *Sentman et al.* [1983] mechanism. In a series of papers *Orlowski et al.* [1990,

Paper number 95JA00062.
0148-0227/95/95JA-00062$05.00

1993] and *Orlowski and Russell* [1991] reopened the analysis of these waves with both statistical as well as selected case studies at Venus and concluded in accordance with *Fairfield* [1974] that the shock is most likely the source of these waves.

One of the very intriguing features characterizing upstream whistlers is their variable spectral shapes observed in the spacecraft frame. While right-hand (RH) polarized spectra are broad, monotonically decreasing between 1 and 3 Hz, the left-hand (LH) polarized spectra always have a sharp peak at frequencies between 1 and 2 Hz and a strong cutoff of 150-200 dB per decade between the peak and the Nyquist frequency. (See *Fairfield* [1974] and *Orlowski and Russell*, [1991] for details.) Such a cutoff is sharper than the cutoff due to the instrumental antialiasing filter of the ISEE magnetometer and occurs well below its 3-dB corner frequency [*Russell*, 1978]. *Fairfield* [1974] correctly identified such different spectra as being caused by the same wave mode, namely by the whistler mode. However, he did not provide a detailed explanation how such a spectrum can be formed in the spacecraft frame. In order to explain the behavior of these spectra *Orlowski et al.* [1993] proposed that the observed spectral shape can be the result of unusually large negative Doppler shift combined with the dispersive properties of a broadband $\Delta\omega/\omega \approx 1$ whistler mode. They also indicated that an apparent peak in the spectra of RH waves is most likely a "break" between superimposed spectra of waves from two different sources, propagating in different modes. Moreover, they concluded that the apparent sharp peak (local maximum) commonly observed in the LH spectra may not exist at all in the plasma frame. *Orlowski et al.* [1993] suggested that such a peak is likely to be caused by so-called "band edge" effects below the Nyquist frequency. They also indicated that the original spectra of whistlers must have a power law-like shape in order to account for the observed spectral variability.

This paper aims to resolve the question of the variability, formation of the spectral shapes, and observed polarizations of upstream whistlers as well as address the thus far controversial question of the generation and damping of whistlers in the upstream region. In section 2.1 we discuss electron dynamics and instabilities that may be relevant to the generation of the whistlers within the shock ramp. In sections 2.2, 2.3 and 2.4 assuming a power law-like spectral form, we derive a fitting procedure and calculate plasma frame power spectral densities for two cases. In the section 3.2 we present the results of the detailed fitting of the upstream electron distribution functions in the Earth's foreshock using a seven drifting bi-Maxwellian fit as well as the results of calculations of linear damping rates using Vlasov theory for the same two cases in order to examine how the fine structure of the suprathermal electron distribution influences the dispersive properties of upstream whistlers. Further, (sections 3.1 and 3.2) we discuss and compare convective damping lengths calculated from theory with the attenuation lengths derived from ISEE magnetic field data. We also discuss the results of the fitting procedure and compare the resulting spectral shapes to those observed within the shock. In section 4 we discuss and interpret all the theoretical and experimental work relevant to the generation of upstream whistlers in the view of the results on damping reported in this paper. The theoretical calculations are carried out using a kinetic solver, newly developed by *Krauss-Varban et al.* [1994], which uses no approximations except for those stemming from numerical accuracy requirements. Throughout the paper we will be using following symbols:

ω	wave angular frequency;
γ	growth/damping rate;
Ω_p	local proton gyrofrequency;
Ω_e	local electron gyrofrequency;
ω_{LH}	lower hybrid frequency;
c/ω_p	proton inertial length;
c	speed of light;
$D(\omega,\mathbf{k})=0$	full electromagnetic dispersion relation derived from linear Vlasov theory;
Φ	cross-shock electric potential;
$\mathbf{n}$	shock normal vector;
$\Delta\delta$	shock thickness;
V_r	resonant velocity;
$k_{\parallel}$	parallel wave number;
k_{perp}	perpendicular wave number;
$\mathbf{k}$	wave vector;
V_g	group velocity;
V_f	flow velocity;
λ	wavelength;
Λ_c	convective damping length;
η	Heaviside function;
f_{Ny}	Nyquist frequency (in Hertz);
S_{xx}	power autospectral density (in square nanoteslas per Hertz);
$\mathbf{S}$	spacecraft separation vector;
τ	time lag;
$\mathbf{B}_o$	background magnetic field;
n	normal coordinate within the shock ramp;
n_p	proton density;
V_{sw}	velocity of solar wind;
Θ_{Bk}	propagation angle;
Θ_{kV}	angle between the solar wind flow and the wave vector;
Θ_{Bn}	angle between the magnetic field and shock normal;
MA	Alfvenic Mach number;
V_{sc}	spacecraft velocity.

2. Spectral Formation of Upstream Whistlers

2.1. Electron Dynamics and Instabilities Relevant to Whistler Generation

In this subsection we examine a variety of the electron-involving processes within the shock ramp that may be relevant to the generation of upstream whistlers. We note here that many mechanisms may be responsible for generation of whistler waves, that is, shock front perturbation, proton temperature anisotropy, beam and ring distributions, etc. These mechanisms are currently under investigations [*Krauss-Varban et al.* 1994]. However, we focus here mainly, but not exclusively, on electron dynamics, which we believe may play a role. The electron dynamics within the shock transition region has been a subject of intensive experimental research by *Anderson* [1974], *Anderson et al.* [1979], *Bame et al.* [1979], *Feldman et al.* [1982], *Gosling et al.* [1989], *Scudder et al.* [1986], *Schwartz et al.* [1987, 1988], *Thomsen et al.* [1983, 1985, 1987], and others. Despite valuable theoretical efforts by *Wu* [1984], *Tokar and Gurnett* [1984, 1985], *Scudder et al.* [1986], *Krauss-Varban and Burgess* [1991],

Krauss-Varban and Wu [1989], *Liewer et al.* [1991], *Veltri et al.* [1990], *Veltri and Zimbardo* [1993a, b], and others involving analytical or Monte Carlo calculations of distribution functions, test particle approaches, or full particle simulations, the details of electron dynamics have not been satisfactorily addressed to date.

The main research focus has been placed on electron heating within the ramps of shocks with different Mach numbers and plasma betas [*Feldman et al.*, 1983; *Scudder et al.*, 1986; *Friedman et al.*, 1990; *Gosling et al.*, 1988, and references therein]. The results of investigating such a process in the deHoffmann-Teller frame [*Schwartz et al.*, 1988; *Krauss-Varban et al.*, 1991] indicate that the heating of electrons occurs through microdissipation of the cross-shock potential energy [*Gary* 1987], since the calculated effective heating seems to correlate with the bulk flow velocity as observed by *Thomsen et al.* [1987]. For resistive shocks the microdissipation is likely to be accomplished through current-driven ion-acoustic instability [*Onsager and Thomsen*, 1991]. For dispersive shocks *Balikhin and Gedalin* [1993] proposed a so-called electron trajectory nonlinear instability. Only recently has *Krauss-Varban* [1992] performed a hybrid and full particle simulations that included kinetic "halo" electrons. His results indicate that anisotropy-driven instabilities may play an important role in electron heating as well as in exciting whistlers within the shock ramp. Additional studies of even more relevant two-dimensional (2-D) full kinetic simulations of the shock with subproton length scale resolutions and realistic mass ratios are currently being undertaken [*Pantellini et al.*, 1993]. Below, we focus on a simplified picture of electron dynamics involving simple resonances.

Electrons enter the shock ramp where a fraction of the very large pitch angle electrons reflect quasi-adiabatically [*Feldmann et al.*, 1983] and together with some fraction of the hot field aligned electrons leaking from the magneto-sheath [*Gosling et al.*, 1989] return back upstream forming a loss cone-like distribution [*Feldman et al.*, 1983] or nongyrotropic distribution in the shock foot, both unstable for oblique whistler waves [*Veltri and Zimbardo*, 1993a]. The bulk of the electron (and proton) population enter deeper into the shock ramp and encounter (1) the electric field associated with cross-shock potential, $\mathbf{E}_n(n) = -\partial\Phi/\partial\mathbf{n}$; (2) transverse (motional) electric field $\mathbf{E}_t(n) = -\mathbf{V}_f(n) \times \mathbf{B}(n)$; and (3) transverse magnetic field gradient and curvature drift fields, which combined provide free energy for resonantly excited waves by producing electron beams and/or temperature anisotropy. The large compression and rotation of the magnetic field within the ramp enables more electrons to reach one of the cyclotron resonant conditions defined by $(\omega - m\Omega_p(n))/k_{\parallel} = V_r(n)$ (Landau resonance for m equal 0) where n is the coordinate along the shock normal, and generate finite band whistler waves, which are obliquely propagating along or against the flow [*Tokar and Gurnett*, 1984]. The above-mentioned transverse fields and ensuing differential drifts cause electrons and protons to resonate ($k_{perp}V_r \approx \omega$) and produce electrostatic lower hybrid waves at frequencies around the local $\omega_{LH} \approx (\Omega_p(n)\,\Omega_e(n))^{1/2}$ [*Gary*, 1987]. These are Doppler shift broadened and propagate at maximum within a few degrees of the perpendicular direction. The lower hybrid instability [*Timofeev and Pistunovich*, 1970] is known to effectively heat electrons and is responsible for generation of electrostatic waves observed at the shock [*Vaisberg et al.* 1983 and *Mellot and Greenstadt*, 1988]. However, these waves are unlikely to contribute to electromagnetic emissions observed at the shock.

2.2. Expected Spectral Form and Frequency Range

In the previous section we briefly discussed the electron dynamics within the shock ramp and indicated that as a result of the shock cross-field drifts, protons and electrons may become unstable to whistler emissions. Now we attempt to deduce the expected spectral properties of such unstable whistlers that may be observed within the shock ramp and upstream. There is an important distinction between the wide range of whistlers that may possibly be generated in the shock ramp, for example, by mechanisms described in the previous section, and those that actually can be observed. The most likely observable waves are those which are able to grow to amplitudes above the noise or the sensivity level of the measuring instrument. The observability of these waves depends not only on the mode properties, such as frequency and growth rate, but also on the thickness of the shock and on the location and time spent by the waves in the unstable region. We postulate that the minimum observed frequency corresponds to whistler waves that undergo a single oscillation as they are convected through the shock layer. The narrow frequency band of the group-standing whistlers will reach saturation and contribute to electro-magnetic noise within the shock transition [*Gurnett*, 1985]. In the case when $|\mathbf{V}_g.\mathbf{n}| > |\mathbf{V}_f.\mathbf{n}|$ and $\omega/\Omega_p >> MA$, lower frequency waves (of longest wavelengths, λ, up to the shock thickness, $\Delta\delta$) spend more time within the unstable region, while higher frequencies spend a shorter amount of time there because they have higher group velocities and leave the growth region faster. The expected spectral shape is characterized by higher spectral densities for lower frequencies and lower spectral densities for the waves close to the upper limit of the escaping frequency band. Just upstream of the shock the upper edge of this frequency band is defined by the fastest waves that still were able to grow to a strength substantially above the sensivity threshold of our measurements. However, their contribution to the spectra will diminish as the wave propagates upstream, since those higher frequency and smaller wavelength waves are more prone to strong damping [*Gary and Mellott*, 1985]. This effect of the increase of the damping rate with increase of the wave number will be shown and discussed in section 3.2. Although we do not present a detailed analysis of the spectral dependency of the damping along the ray path, our observations of many cases of upstream whistlers [*Orlowski et al.*, 1993] clearly indicate that the highest frequencies (in the plasma frame) are always observed closest to the shock and diminish faster than lower frequencies away from the shock.

2.3. Fitting Power Law Plasma Frame Spectra

We assume here that the average spectral density of the upstream whistlers in the plasma frame can be well approximated by a power law of the form $S_{xx} = a/\omega^q$; $q>1$, where a, q, ω_1 (lower frequency cutoff) and $\Delta\omega = \omega_2 - \omega_1$ are the fitting parameters. The wave power at frequency ω within the frequency band $\delta\omega << \Delta\omega$ has the form

$$P_{xx}(\omega, \delta\omega) = \int_{\omega - \delta\omega/2}^{\omega + \delta\omega/2} S_{xx}(\nu)\, d\nu =$$

$$\frac{\omega}{2^{1-q}(q-1)} S_{xx}(\omega)\left[\left(2 + \frac{\delta\omega}{\omega}\right)^{1-q} - \left(2 - \frac{\delta\omega}{\omega}\right)^{1-q}\right] \qquad (1)$$

In the spacecraft frame the corresponding power will be

$$P_{xx}(\omega' + \delta\omega') = \int_{\omega' - \delta\omega'/2}^{\omega' + \delta\omega'/2} S_{xx}(\nu')\, d\nu' = \langle S_{xx}(\omega') \rangle \delta\omega' \quad (2)$$

where $\langle S'_{xx}(\omega') \rangle$ is an estimate of the spectral density in the spacecraft frame, and $\delta\omega'$ is a Doppler-shifted bandwidth. Also, the Doppler shift and dispersion relation have form

$$\omega' = \omega + \mathbf{k} \cdot \mathbf{V}_f \quad (3)$$

$$D(\omega, \mathbf{k}) = 0 \quad (4)$$

Since the wave power is invariant for a Doppler-shift transformation, (1) equals (2), the solution of (1)-(4) allow us to evaluate the spectral shape $\langle S'_{xx}(\omega') \rangle$ in the space-craft frame in the following way: first, we set arbitrarily a plasma frame frequency ω and $\delta\omega$ and solve (4) for k using measured Θ_{Bk} and Θ_{kV}; then we apply k to calculate ω' and $\delta\omega'$. Using these quantities and the power conservation law we calculate $\langle S'_{xx}(\omega') \rangle$.

However, the spectral density $\langle S_{xx}(\omega') \rangle$ is not what is in reality observed. This is due to the fact that commonly used spectral analysis techniques such as power spectra from the fast Fourier transform (FFT) assume a symmetric spectrum and do not discriminate between different polarizations of the wave. In fact, the spectral form is two-sided and non-symmetric in the spacecraft frame and is polarization dependent. The calculated "observed" space-craft frame power spectral density $\langle S'_{xx}(\omega'') \rangle_{obs}$ $\omega'' \geq 0$ expressed by

$$\langle S'_{xx}(\omega'') \rangle_{obs} = [\eta(\omega') \langle S'_{xx}(\omega') \rangle]_R + [\eta(-\omega') \langle S'_{xx}(\omega') \rangle]_L$$

can now be fitted to the measured spectra.

The above formula describes the fact that the measured mixed polarization spectrum in the spacecraft frame is created by overlapping two spacecraft frame spectra with opposite polarizations, indicated by R (right-handed) and L (left-handed). As a consequence, the observed spectrum cannot be exactly mapped back into the plasma frame.

The solution of the dispersion relation used in (4) is described by *Krauss-Varban et al.* [1994], and the distribution functions used for calculation of $D(\omega, \mathbf{k})$ are described in the section 3.2 of this paper. The direction of propagation $\mathbf{k}/k$ of the upstream whistlers was derived using minimum-variance technique [*Hoppe et al.*, 1982] assuming consistent with observations [*Orlowski and Russell*, 1991] that upstream whistlers are approximately planar waves. Hence we consider the direction of minimum variance of magnetic field as an estimate of unit vector parallel to the wave vector.

2.4. The Results of Fitting of Plasma Frame Spectra

Here we present the results of fitting of the plasma frame spectra (using the four parameters a, q, ω_t, and $\Delta\omega$) to the upstream whistler spectra obtained from FFT of the magnetic field time series measured on board the ISEE 1 spacecraft. We note here that the propagation angle of the observed upstream whistlers which we take for our calculations is constant at least within $\omega''_{peak} \pm \delta\omega''$ where most of the power resides. Therefore we use for our fit a single propagation angle determined at $\omega'' \approx \omega''_{peak}$. We show the results of the application of this procedure to two cases of predominantly (but not exclusively) RH and LH observed polarizations.

Case 1. In Figure 1 we show an example of the dynamic spectrum of the magnetic field component of predominantly RH waves as recorded by ISEE 1. The spacecraft crossed the shock at about 2313:30 UT on July 22, 1978. The upstream whistlers are observed upstream of the shock leaving the shock foot at 2314:30 UT and propagating upstream until the end of the displayed record at 2322:30 UT. There are clearly seen, relatively broadband wave emissions between 1 and 4 Hz. We note that the apparent fluctuation of the intensity of the spectra may result from a variable contribution to the wave power from sources located at the shock surface but at different relative locations from the spacecraft crossing point. Enhancements of the wave power are caused by contributions from waves generated at the shock, by sources located closest to the spacecraft along their corresponding ray paths. Figure 2 shows the result of the fitting procedure for this case using the spectrum observed between 2316 and 2318 UT on July 22, 1978. Plasma and wave parameters we used are the following: V_{sw}= 355 km/s; Θ_{Bk} =31°; Θ_{kV}=63°; B_o=8.4 nT; n_p= 9 cm^{-3}; and T_p =15.5 eV. The lighter shaded spectrum is the spacecraft frame spectrum that fits to the observed spectrum (indicated by solid circles) starting at about 2 Hz at the evident break in the observed spectrum between the low-frequency part of the spectrum with the relatively flat slope $q < 2$ per decade and the steep spectrum with $q = 7$. Careful inspection of Figure 2 shows that the upstream plasma frame frequency corresponding to this break is about 4 Hz. The whistlers with such a frequency (escaping frequency) are the slowest (with longest wavelength and largest amplitude) waves that were able grow and to leave the shock against the flow.

Case 2. In Figure 3 we show an example of a dynamic spectrum of the magnetic field component of predominantly LH waves as recorded by ISEE 1. The spacecraft crossed the shock from the upstream region at about 2028:30 UT on December 15, 1977. The waves are observed upstream of the shock from 2019:30 UT to the shock foot at 2026:30 UT. In contrast to the RH case the emissions are relatively narrow band between 0.6 and 1.1 Hz. Again, small fluctuations of the intensity are present due to the spatially extended source of the waves at the shock surface. A noticeable shift to the higher frequencies seen at about 2020:30 UT is due to the sudden change in proximity of the strongest source magnetically connected to the spacecraft, due to a rotation of the interplanetary magnetic field (IMF). Figure 4 shows the result of the fitting procedure for this case using the spectrum observed between 1953 and 1955 UT on December 15, 1977. Plasma and wave parameters were V_{sw} =330 km/s; Θ_{Bk} =31°; Θ_{kV}= 17°; B_o = 4.3 nT; n_p = 5 cm^{-3}; and T_p = 13.0 eV. The lighter shaded spectrum indicates the spacecraft frame spectrum that fits to the observed spectrum (indicated by solid circles). The sharp peak and cutoff of the observed spectrum is well represented. In contrast, the plasma frame spectrum (dark shade) is monotonic with a spectral density slope of, q=5.6. In this case the lower edge of the frequency band in the plasma frame (escaping frequency) is equal to about 2 Hz. We want to emphasize here that the above fitting procedure leads to an

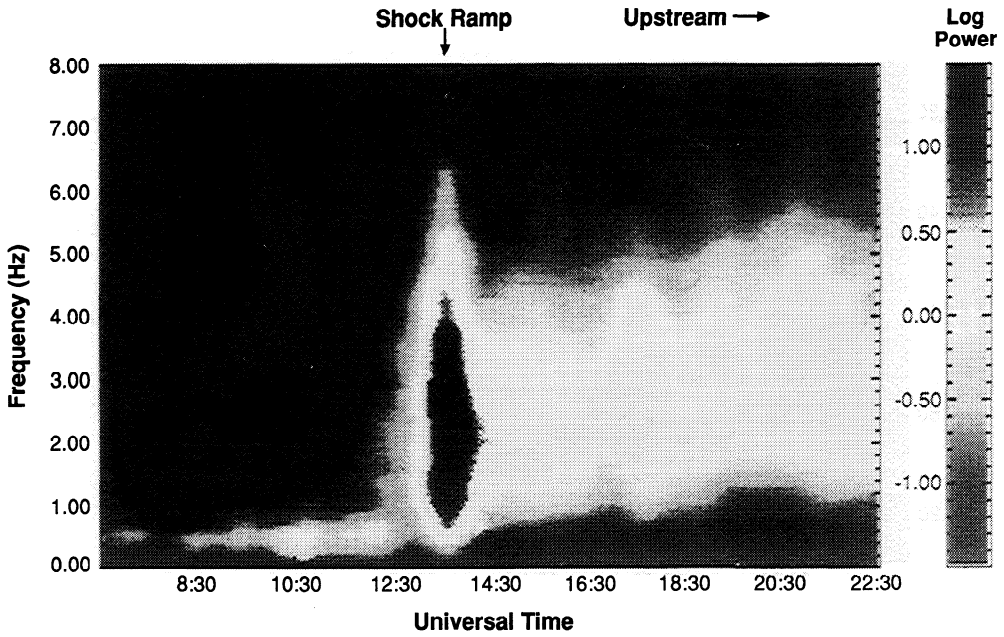

Figure 1. Dynamic spectrum of magnetic field fluctuations in the vicinity of the shock. The upstream whistlers are seen between 2314:30 and 2322:30 UT on July 22, 1978. The horizontal scale shows minutes after 2300 UT.

unambiguous determination of the shape and location of the plasma frame spectra. This is because we fit not only the total power but also the edge of the frequency band which is determined by the break for RH and by the cutoff for LH spectra, respectively.

3. Determination of Damping Properties of Upstream Whistlers

3.1. Experimental Evaluation of Amplitude Attenuation Length

In this section we describe our method of evaluating the attenuation length ΔL_c of the upstream whistlers propagating along magnetic field line based on simultaneous two- spacecraft measurements. In the next section we will explain the calculation of the convective damping length Λ_c from linear Vlasov theory which then will be compared to ΔL_c. First of all we want to note that the major difficulty is determining the exact direction of IMF field lines and the motion of the shock front at times of measurements conducted farther upstream and consequently at the location of the source of wave packets arriving at the observation site. In order to evaluate ΔL_c we first determine the shock velocity as $V_{sh} = \mathbf{S} \cdot \mathbf{n}/\tau$, where $\mathbf{S}$ is the spacecraft separation vector, $\mathbf{n}$ is a unit vector parallel to the shock normal, and τ, is the time lag between two spacecraft obtained from correlation analysis [*Hoppe et al.*, 1981]. Correcting for the spacecraft velocity in the plasma rest frame, an estimate ΔL_c of convective damping length is calculated from the following formulas:

$$\Delta L_c = | L_{cf}^* - L_{ci}^* | ;$$

$$L_{ci}^{*2} = L_{ci}^2 + V_{sw}^2 \sin^2\Theta_{vn} (L_{ci}/V_{gu})^2 - 2L_{ci} V_{sw} (L_{ci}/V_{gu}) \sin\Theta_{vn} \sin\Theta_{Bn};$$

$$L_{cf}^{*2} = L_{cf}^2 + V_{sw}^2 \sin^2\Theta_{vn} (L_{cf}/V_{gu})^2 - 2L_{cf} V_{sw} (L_{cf}/V_{gu}) \sin\Theta_{vn} \sin\Theta_{Bn};$$

$$L_{cf} = [\{\mathbf{V}_{sc}.\mathbf{n} - V_{sh}\}(t_f - t_i) + \{\mathbf{V}_{sc}.\mathbf{n} - V_{sh}\}(t_i - t_o)]/\cos\Theta_{Bn};$$

$$L_{ci} = [\mathbf{V}_{sc}.\mathbf{n}(t_i - t_o) - V_{sh}(t_i - t_o)]/\cos\Theta_{Bn};$$

where $\mathbf{V}_{sc}$ is spacecraft velocity; V_{sh} is shock velocity at the time of shock crossing; V_{gu} is a whistler average group velocity along

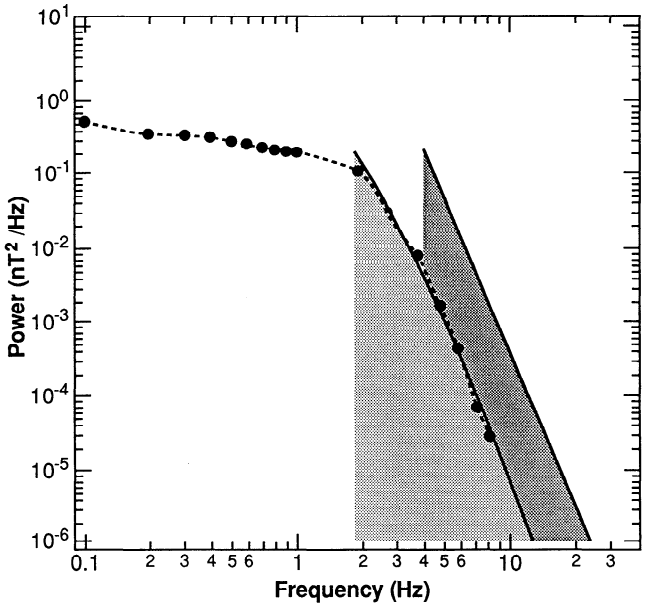

Figure 2. Plasma frame (fitted) spectrum (dark gray), calculated, observed spectrum (light gray) and measured spectrum of upstream whistlers within the time interval between 2316 and 2318 UT on July 22, 1978.

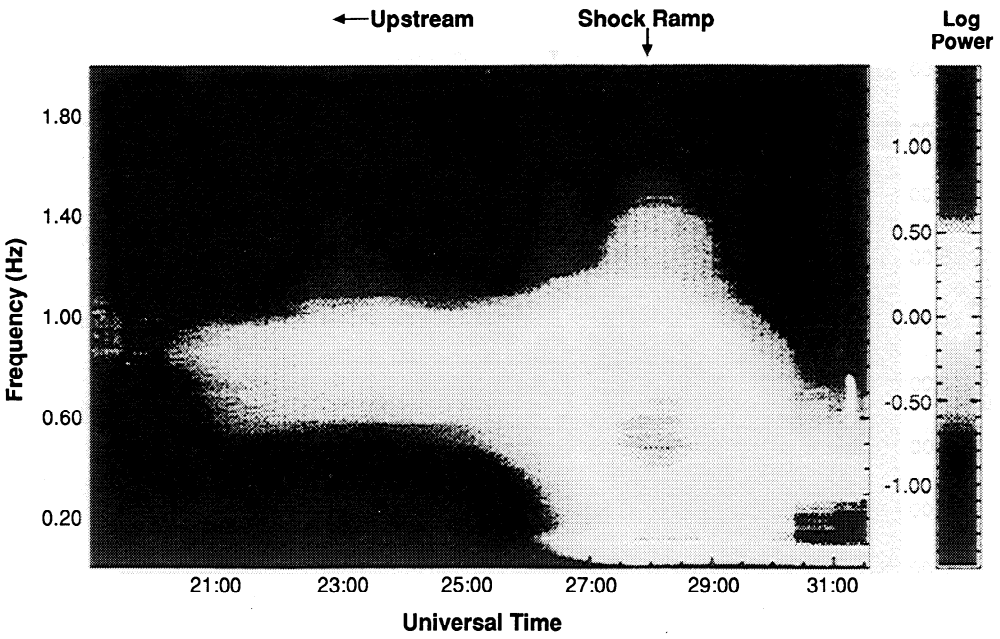

Figure 3. Dynamic spectrum of magnetic field fluctuations in the vicinity of the shock. The upstream whistlers are seen between 2019:30 and 2026:30 UT on December 15, 1977. The waves are predominantly LH in spacecraft frame. The horizontal scale indicates minutes after 2000 UT.

the magnetic field line; Θ_{Bn} is the angle between shock normal and magnetic field; and t_0 is the shock crossing time. The integrated power over the whistler spectrum $P(t)$ must satisfy the following condition: $\ln [P(t_i)/P(t_f)] = 1$, where t_i is initial time; t_f is final time of observations; L_{ci} (L_{cf}) is a distance from the wave source to the spacecraft along magnetic field line at time t_i, (t_f), and ΔL_c is a attenuation length corrected for convection of wave packet along the field aligned ray path from the source on the shock surface up to the observation site. The above approximation is valid under the following assumptions: (1) Shock speed along $\mathbf{B}_0$ and shock normal direction at the time of the observation is the same as during the shock crossing (some time earlier). (2) Ray paths of upstream whistlers are field aligned. In fact, *Orlowski and Russell* [1991] showed that group velocities of upstream whistlers are within 10° of the $\mathbf{B}_0$, moreover, the uncertainty associated with the variable motion of the shock may be comparable to the error produced by the approximation of field aligned ray paths. (3) The time of flight

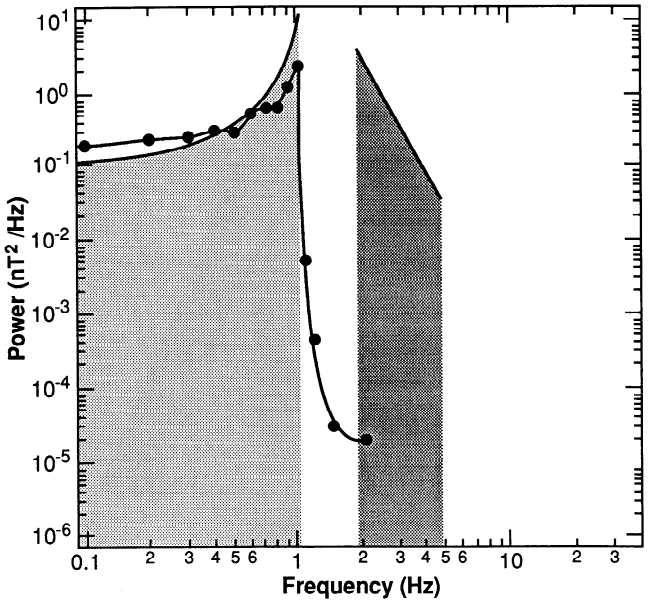

Figure 4. Plasma frame (fitted) spectrum (dark gray), calculated, observed spectrum (light gray), and measured spectrum of upstream whistlers between 1953 and 1955 UT on December 15, 1977. The waves are predominantly LH in spacecraft frame.

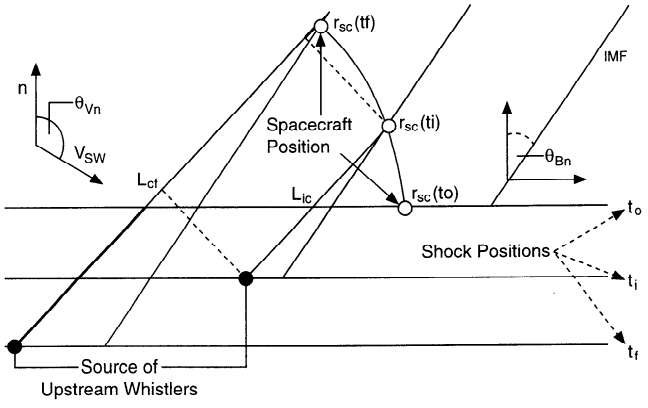

Figure 5. The geometry used for calculations of the power e fold attenuation length from ISEE data. The open circles indicate spacecraft position r_{sc} at times t_0 (shock crossing time) t_i (initial time) and t_f (final time). L_{ci} is the initial distance from the source of the waves (solid circle), and L_{cf} is the final distance from the source of the waves (solid circle); both are calculated taking into account the convection of solar wind. The bolded part of L_{cf} is an e folding attenuation distance $\Delta L_c = | L^*_{cf} - L^*_{ci} |$. The value Θ_{Bn} is an angle between IMF and shock normal, and Θ_{vn} is an angle between solar wind velocity and the shock normal. Relevant shock positions are also indicated.

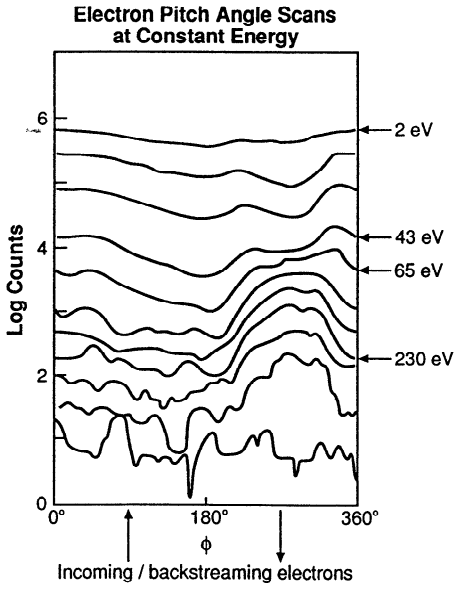

Figure 6. The observed electron flux pitch angle distribution between 2316 and 2318 UT on July 22, 1978.

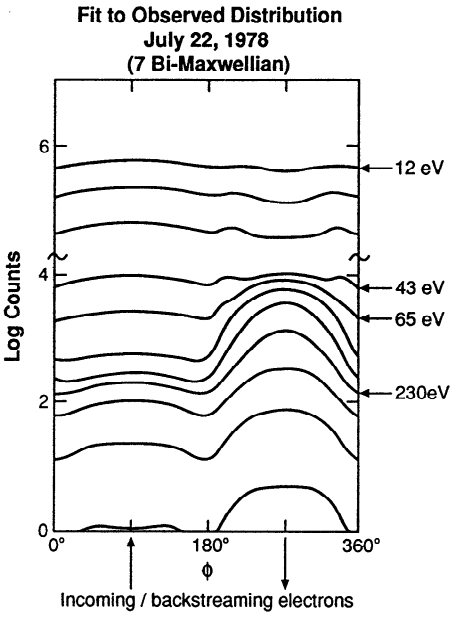

Figure 7. The fitted electron flux pitch angle distribution of Figure 6 using seven bitemperature Maxwellian fit (case 1). The relative direction of the electrons with respect to the magnetic field is also indicated.

effect is small but finite, for examples, $V_{sh}.\mathbf{b}_o << V_{gu}$, $\mathbf{V}_{sc}.\mathbf{b}_o << V_{gu}$, and $\Delta L_{cf}/V_{gu} << t_f - t_i$ which is commonly satisfied for upstream whistlers at Earth since their group velocities reach 200 to 400 km/s or more in the spacecraft frame. By varying the initial time t_i and assuming a 15% variability of V_{sh} (between the time of the measurement of V_{sh} and the observation of waves) we find following ranges of attenuation length estimate: case 1, (July 22, 1978, 2315-2318 UT) ΔL_c^* = 1160 to 2070 km, case 2, (December 15, 1977, 1953-1955 UT) ΔL_c^* = 150 to 260 km. The geometry used in calculations of ΔL_c is shown in Figure 5.

3.2. The Results of Calculation of Convective Damping Lengths

As we mentioned in the introduction, the damping properties are very important for distinguishing between local and shock generation of the waves. We note that the *Sentman et al.* [1983] hypothesis requires that the observed wave be unstable for the observed electron distribution. Specifically, they point toward a slightly suprathermal large pitch angle particle population as the source of free energy for the Landau resonance based instability. On the other hand, the shock generation hypothesis assumes a stable foreshock plasma. Since the waves can be considered as small amplitude waves $\delta B/B \leq 0.1$, the observed damping scales should be consistent with those calculated from linear Vlasov theory.

In order to calculate damping rates we use plasma and wave parameters assuming a Maxwellian proton distribution. The most difficult problem was to fit the fine structure of the electron distribution function obtained by the ISEE spacecraft [*Ogilvie et al.*, 1978]. An example of the measured electron distributions in the form of pitch angle flux contours for case 1 is seen in Figure 6. The complicated structure of the back streaming beam at energies at and slightly above the thermal energy is clearly seen. Our aim is to specifically fit the part of distribution that is most likely to interact with the upstream whistlers. In order to achieve good correspondence between observed and fitted electron pitch angle scans we decided to use not a five, like *Sentman et al.* [1983], but a seven drifting bitemperature Maxwellian fit. Using the measured plasma properties and fitted electron distribution function we then solve the full electromagnetic dispersion relation.

Case 1. Figure 7 shows our fit to the measured distribution presented for case 1 in Figure 6. In both of these figures the three lowest energy levels are shifted up (by 1/2, 1, and 1½ decades respectively) for better separation. The results of the linear Vlasov theory calculations making use of this fit and the plasma data are shown in Figure 8. In this Figure the upper panel shows the real part of the dispersion relation calculated in the spacecraft frame, the middle panel shows damping rates, and the lower panel shows the convective damping length as a function of wave number. The damping length is given both normalized by the proton inertial length and in kilometers. The dark shading indicates the bandwidth of the waves as relevant to the observations. The solid lines correspond to the seven drifting bi- Maxwellian fit, and the dashed lines show results for a single Maxwellian. The dispersion relation in the upper panel clearly indicates that the spectrum is dominated by the original polarization of the waves ($\omega > 0$). A potential contribution from Doppler- shifted LH ($\omega < 0$) waves would be at much lower frequencies than the actual observed band. It is also clear that in this case the fine structure of the electron distribution represented by the seven drifting bi-Maxwellian fit does not affect the real part of the dispersion (solid and dashed lines are nearly identical). However, the influence on the growth rate is significant as seen in the middle panel of Figure 8. The existence of the back-streaming beam seems to cause the damping rate to decrease from about 1.4 to 0.4 Ω_p within the upstream wave bandwidth (solid line), which is more than 50% smaller than the damping rate calculated from a single Maxwellian approximation of the electron distribution (dashed line). We note that within the full range of frequencies the upstream whistler waves were found to be stable with significant damping rates. The lower panel of

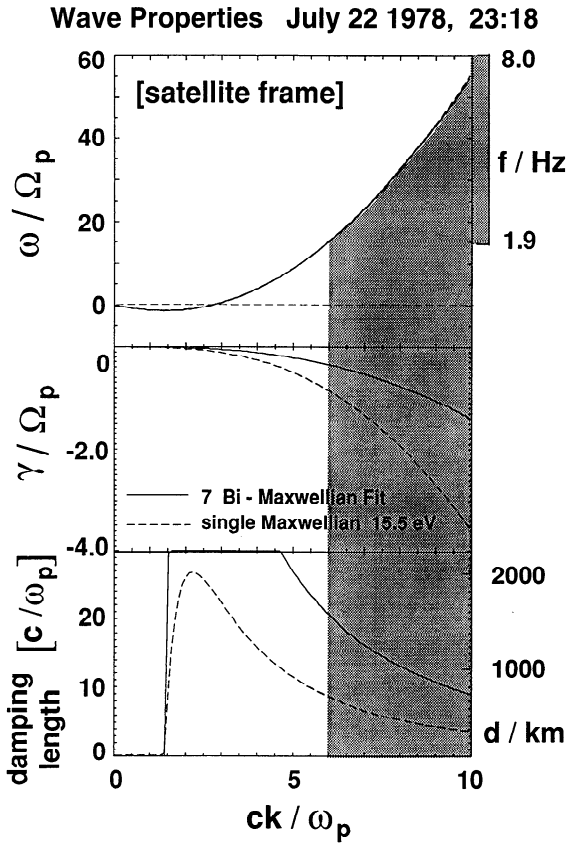

Figure 8. The results of the solution of the full electromagnetic dispersion relation for case 1, for 2316 to 2318 UT on July 22, 1978. The real part of dispersion relation in the spacecraft frame is shown in the upper panel, where the dashed line indicates zero frequency in the spacecraft frame; the imaginary part of the dispersion relation, damping rate, is shown in the middle panel; and convective damping length is shown in the lower panel. The shaded area indicates bandwidth of upstream whistlers.

Figure 8 shows the results of the calculation of the convective damping lengths $\Lambda_c = V_g^*/|\gamma|$. For simplicity we have calculated here the convected group velocity along the wave vector, $V_g^* = \partial\omega/\partial k - \mathbf{V}_{sw} \cdot \mathbf{k}$. Since $\Theta_{Bk} \approx 31°$ for both cases, V_g^* should cause a slight consistent underestimation of convective damping length along the magnetic field line. But given all the un-certainties of the observational determination of ΔL_c mentioned in the previous section the error still possible in Λ_c will be smaller than in ΔL_c. It is clearly seen that Λ_c is very sensitive to the fine structure of the electron distribution. The lower panel of Figure 8 shows that the single Maxwellian fit predicts Λ_c to be in the range of 450 to 600 km, inconsistent with experimental estimates, while the use of the seven drifting bi-Maxwellian fit enables us to correctly predict the Λ_c ranging from 800 to 1600 km. The ability of linear Vlasov theory to correctly predict Λ_c for these small amplitude whistlers strengthens our conclusion about the stability of the waves based on linear theory versus local growth.

Case 2. Again we use the plasma parameters as above and assume a Maxwellian proton distribution with temperature of T_p=13 eV. The measured electron distributions in the form of pitch angle flux contours for case 2 is shown in Figure 9, and our fit is shown in Figure 10. Again, in both Figures the lowest three energy levels are upshifted by consecutive steps of 1/2 decade. The dashed lines in Figure 10 indicate that no attempt has been made to match these to the observed levels, which for the two lowest energies can be shown to originate from photoelectrons [*Feldman et al.*, 1983]. Using the measured plasma properties and the fitted electron distribution function we again solve the full electromagnetic dispersion relation. The results are shown in Figure 11. The dark shading indicates the bandwidth of upstream whistlers as relevant to the wave data for case 2. The dispersion relation (upper panel) clearly indicates that the spectrum is dominated by LH waves. Note that the threshold for finite (positive) group velocity matches well with the observed cutoff of the waves at approximately 1 Hz. It is also clear that the fine structure of the electron distribution affects the real part of the dispersion only slightly in this case. Also, the effect on the growth rate seems not to be as significant as in case 1. The overall damping rate, however, ranges from about -5 to -1 Ω_p within the wave band. We note that also for this case within the full range of frequencies the upstream whistlers were found to be significantly damped. The lower panel of Figure 11 shows the results of the calculation of Λ_c. As it is clearly seen from this Figure, the single as well as seven drifting bi-Maxwellian fit predicts Λ_c within the range of 120 to 220 km, consistent with derived experimental estimates. Also note that the observed band is indeed that part of the spectrum for which the predicted damping lengths are large. Since the damping increases significantly with wave number, the observed waves should not be contaminated much by RH polarized waves.

It is important to note that pitch angle scans fitted in this paper (see Figures 7 and 10) represent the best fit to the observed distributions (Figures 6 and 9) that we could achieve using a sum of seven drifting bi-Maxwellian electron distributions. Due to the number of features of the distribution that can give rise to damping or growth, it is difficult to provide detailed accuracy analysis. However, it is obvious that our fit reproduces major (associated with larger energy density) as well as minor features of observed spectra more accurately than do fits provided by *Sentman et al.* [1983], which used only five bitemperature Maxwellian components. Also, we would like to point out the

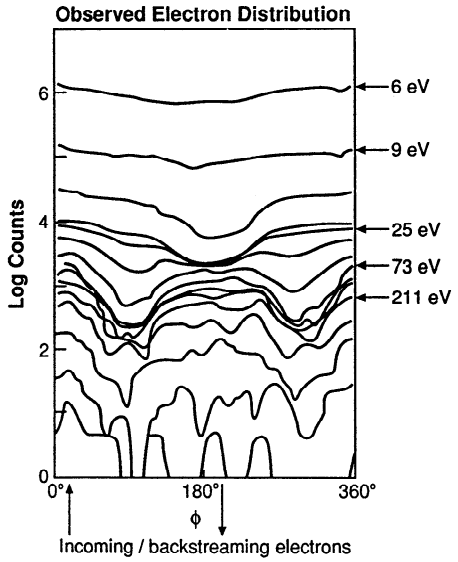

Figure 9. The observed electron flux pitch angle distribution between 1953 and 1955 UT on December 15, 1977.

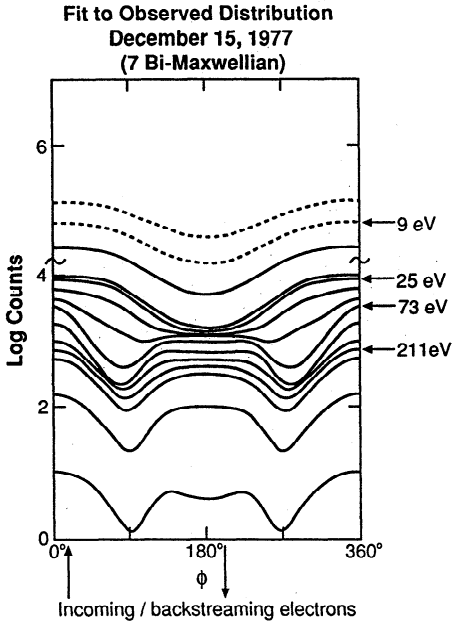

Figure 10. The fitted electron flux pitch angle distribution of Figure 9 using a seven drifting bitemperature Maxwellian fit (case 2). The relative direction of the electrons with respect to the magnetic field is also indicated.

following: while a change of 5-10% in the parameters describing the distribution function has no significant effect on the calculated values of $\omega(\mathbf{k})$ and $\gamma(\mathbf{k})$, the resulting pitch angle/energy distribution would clearly be a less accurate fit to the observed ones. More importantly, even much larger changes in the distribution sustaining major features of the observed electron distribution do not reduce the damping to an extent that growth would result in the frequency region of interest.

3.3. Effective Size of the Unstable Region: Shock Thickness

The observable whistlers (see section 2.2) must have wavelengths comparable to or smaller than the size of the unstable region. Hence the wavelength of the upstream whistlers at the minimum escaping frequency (lower edge in the plasma frame spectrum, 4 Hz for case 1 and 2 Hz for case 2) will then correspond to the lower limit of the effective shock thickness. From Figures 8 and 11 we evaluate the lower limit of the effective shock thickness as 79 and 106 km for case 1 and 2, respectively, which is approximately equal to one upstream proton inertial length. This result is consistent with direct, two-spacecraft measurements of the low-beta supercritical shock thickness as shown by *Farris and Russell* [1993].

4. Discussion

In this paper we fitted spacecraft frame spectral densities derived from assumed power law-like plasma frame spectral densities to the spectra obtained from FFT of the magnetic field returned from ISEE spacecraft for two cases of upstream whistlers. Also we calculated convective damping lengths of these waves in order to examine whether or not upstream electron distributions are unstable to whistler emission of the observed properties.

Spectral fitting. Using spectral fitting of upstream whistlers we obtained the following results: (1) upstream whistlers observed as RH or LH in the spacecraft frame can be fitted with a common finite bandwidth spectral shape, well approximated by a power law, which indicates that they originate from a finite band source; and (2) the fitted plasma frame spectral slopes are 7 and 5.6 for case 1 and 2, respectively. Those slopes are steeper than the average slope of 4 ± 0.5 obtained by *Rodriguez and Gurnett* [1975] from a statistical study. There may be at least two reasons for this apparent discrepancy. First, observations were made at different locations. Since the whistlers with higher frequencies damp faster traveling along the ray path, the spectrum obtained upstream may be steeper than that at the shock. Second, *Rodriguez and Gurnett* [1975] have most of their spectral points above 10 Hz outside of our fitting range. For $q \geq 4$ the power of the waves within the frequency 10-100 Hz will be at least 1000 times smaller than within the adjacent range 1-10 Hz we consider. Therefore the wave particle transport processes may also be different within these two frequency ranges leading to different spectral shapes.

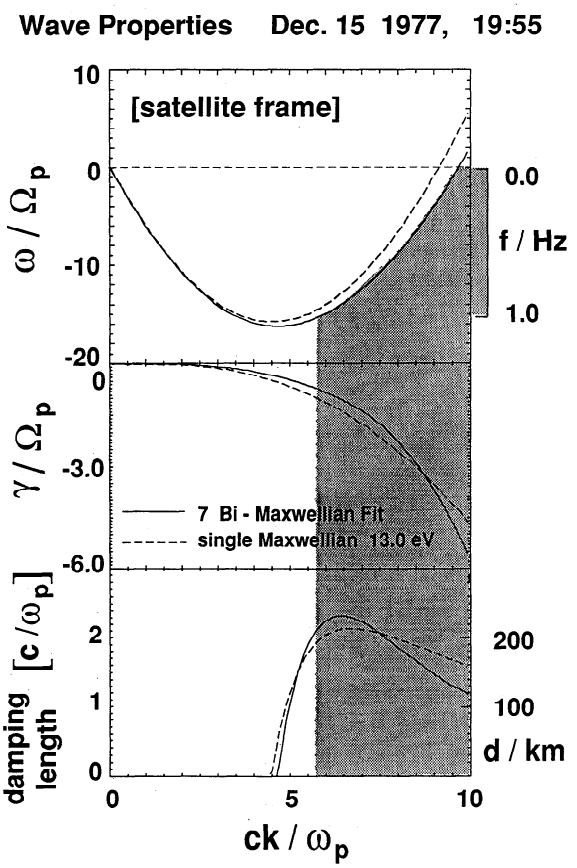

Figure 11. The results of the solution of the full electromagnetic dispersion relation for case 2, for 1953 to 1955 UT on December 15, 1977. The real part of dispersion relation in spacecraft frame is shown in the upper panel, where the dashed line indicates zero frequency in the spacecraft frame is shown in the upper panel; the imaginary part of the dispersion relation, damping rate, is shown in the middle panel and convective damping length in the lower panel. The shaded area indicates bandwidth of upstream whistlers.

Whistler damping. We performed a detailed case study of the damping of upstream whistlers by calculating convective damping lengths from Vlasov theory (using the seven drifting bi-Maxwellian fit) and comparing them to the attenuation lengths derived from data selected for two cases where the localized source of the waves and local planar geometry could be assumed and shock motion could be sufficiently well evaluated. We find that for the upstream whistlers with the observed properties, the fine structure of the electron distribution function around the backstreaming electron beam typically observed in the foreshock may act to increase (case 2) or decrease (case 1) the damping of the waves. These small changes may affect the convective damping length up to about one order of magnitude, allowing whistlers at times to reach such great distances as those observed by *Fairfield* [1974] and *Hoppe et al.* [1981, 1982]. In both cases we find upstream whistlers to be stable or marginally stable within their finite frequency band. We note here that *Sentman et al.* [1983] found two out of three cases of electron distribution functions to fit to the observed electron data to be stable while the third case was found to be unstable only after an attempt to improve the fit to lower energies (at about 10 eV) at the expense of the goodness of the fit to the thermal population, mainly responsible for whistler damping. This difficulty in fitting simultaneously the low- and high-energy parts of electron distribution we encountered as well, but avoided by increasing the number of fitting Maxwellians to seven instead of accepting a decreased quality of the fit. Since the fine structure of the electron distribution function varies greatly with position with respect to the morphological boundaries of the foreshock [*Fitzenreiter et al.*, 1990], the question of whether or not, as in the specific case, the shock-generated whistlers are able to reach far upstream or will be damped near the shock, depends on the details of their complicated ray paths and the electron distribution they encounter.

5. Conclusions

As was shown by *Anderson, [1974], Anderson et al.* [1979], and *Feldman et al.* [1982, 1983], and others a typical electron temperature of solar wind at 1 AU is relatively constant at roughly about 15 to 25 eV (V_e = 2300 to 3000 km/s). Typical phase velocities V_{ph}, of upstream whistlers, on the other hand range from 350 to 450 km/s [*Fairfield*, 1974; *Orlowski and Russell*, 1991]. Therefore if the *Sentman et al.* [1983] hypothesis was correct and the upstream whistlers were being generated by the Landau resonance with slightly suprathermal large pitch angle electrons as they suggest, the waves should typically have propagation angles $\Theta_{Bk} > \arccos(V_{ph}/V_e)$ larger than 80°. This result, however, is inconsistent with the observed propagation angles of the up-stream whistlers in the foreshock which range from 10° to 50° as shown in-dependently by *Fairfield* [1974] and *Orlowski and Russell* [1991]. Moreover, *Orlowski and Russell* [1991] showed that the amplitude of these waves decreases with increasing distance from the shock, in conflict with the *Sentman et al.* [1983] mechanism which considers the whole foreshock as the region of growth. The prediction of maximum growth rate (and therefore maximum amplitudes) at highly oblique angles is yet another apparent inconsistency of the results of *Sentman et al.* [1983] with the observations, which indicate that the amplitude decreases with increasing propagation angle regardless of the location within the foreshock as expected for damped and not for growing waves [*Orlowski and Russell*, 1991]. Finally, in this report we have shown unambiguously, using two detailed case studies, that upstream whistlers constitute wideband emissions with properties consistent with the shock generation. Moreover, while the fine features of the electron distribution function in the foreshock, invoked by *Sentman et al.* [1983], may influence whistler dispersive properties, they do not result in instability but rather in moderating the Landau damping of the whistler waves with the observed properties. In conclusion, the statistical results of the upstream whistler wave analysis (*cf. Fairfield* [1974], *Orlowski and Russell* [1991], and *Orlowski et al.* [1993], taking into account the properties of upstream electrons [*Feldman et al.*, 1982, 1983] and the results of detailed case studies presented in this paper, clearly indicate that upstream whistlers are generated near the shock rather than by a resonant process in the foreshock. This conclusion is reinforced by the finding that the lower frequency cutoff in the plasma frame is apparently determined by the shock ramp thickness.

Acknowledgments. We thank referees for their helpful comments and suggestions. This work was supported by the National Aeronautics and Space Administration under research grant NAGW-2886 at UCLA and grant NAG5-1492 of the Space Physics Theory Program at UCSD. The work at LANL was conducted under the auspices of the U.S. Department of Energy and supported in part by the NASA SR&T program through work order 18,061. Computational facilities were provided by NSF San Diego Supercomputer Center.

The Editor thanks P. Veltri and J. V. Olson for their assistance in evaluating this paper.

References

Anderson, K. A., Intensity and energy spectrum of electrons accelerated in the Earth's bow shock, *J. Geophys., 40,* 701-711,1974.

Anderson, K. A., R. P. Lin, F. Martel, C. S. Lin, G. K. Parks, and H. Reme, Thin sheets of energetic electrons upstream from the Earth's bow shock, *Geophys. Res. Lett.*, 6, 401-405, 1979.

Arthur, C. W., R. L. McPherron, and J. D. Means, A comparative study of three techniques for using the spectral matrix in wave analysis, *Radio Sci., 11,* 10,833-10,845, 1976.

Balikhin, M. A., and M. Gedalin, Role of small-scale non-linear electromagnetic structures in electron heating, *Rep. WPP-047,* pp.105-108, Eur. Space Agency, Neuilly, France, 1993.

Bame, S. J., et al., High temporal resolution observations of electron heating at the bow shock, *Space Sci. Rev., 23,* 75-97, 1979.

Fairfield, D.H., Whistler waves observed upstream of collisionless shocks, *J. Geophys., Res., 79,* 1368-1378, 1974.

Farris, M. H., and C. T. Russell, Dual spacecraft analysis of waves associated with low beta shocks, *Rep, WPP-047,* pp.259-262, Eur. Space Agency, Neuilly, France, 1993.

Feldman, W. C., et al., Electron heating by field-aligned free energy within the Earth's bow shock, *Phys. Rev, Lett., 49,* 199-209,1982.

Feldman, W.C., et al., Electron velocity distribution near the Earth's bow shock, *J. Geophys., Res., 88,* 96-110, 1983.

Fitzenreiter, R. J., J. D. Scudder, and A. J. Klimas, Three-dimensional analytical model for spatial variations of the forshock electron distribution function: Systematics and comparison with ISEE observations, *J. Geophys. Res., 95,* 4155-4169, 1990.

Friedman, M. A., C. T. Russell, J. T. Gosling, and M. F. Thomsen, Noncoplanar component of the magnetic field at low Mach number shock, *J. Geophys. Res.*, *95*, 2441-2449, 1990.

Gary, S. P., R. L. Tokar, and D. Winske, Ion/ion and electron/ion cross-field instabilities near the lower hybrid frequency, *J. Geophys. Res.*, *92*, 10029-10038, 1987.

Gary, S. P., and M. M. Mellott, Whistler damping at oblique propagation: Laminar shock precursors, *J. Geophys. Res.*, *90*, 99-104, 1985.

Gosling, J. T., D. Winske, and M.F. Thomsen, Noncoplanar magnetic fields at collisionless shocks: A test of a new approach, *J. Geophys. Res.*, *93*, 2735-2744, 1988.

Gosling J. T, M. F. Thomsen, S. J. Bame, and C. T. Russell, Suprathermal electrons at Earth's bow shock, *J. Geophys. Res.*, *94*, 10011-10025, 1989.

Greenstadt, E. W., et al., Whistler mode wave propagation in the solar wind near the bow shock, *J. Geophys. Res.*, *86*, 4511-4516, 1981.

Gurnett, D. A., Plasma waves and instabilities, *Collisionless Shocks in the Heliosphere: Reviews of Current Research*, in *Geophys. Monogr. Ser.*, vol. 35, edited by B. T. Tsurutani and R. G. Stone, pp.207-224, AGU, Washington, D.C., 1985.

Hoppe, M. M., C. T. Russell, L. A. Frank, T. E. Eastman and E. W. Greenstadt, Upstream hydromagnetic waves and their association with backstreaming ion population: ISEE 1 and 2 observations, *J. Geophys. Res.*, *86*, 4471-4492, 1981.

Hoppe, M. M., C. T. Russell, L. A. Frank, T. E. Eastman, and E. W. Greenstadt, Characteristics of the ULF waves associated with upstream ion beams, *J. Geophys. Res.*, 87, 643-650, 1982.

Holzer, R. E., T. G. Northrop, J. V. Olson, and C. T. Russell, Study of waves in the Earth's bow shock, *J. Geophys. Res.*, *77*, 2264-2273, 1972.

Krauss-Varban, D. Simulation of electron acceleration at collisionless shocks, American Institute of Physics Conference Proceedings, 264, *Particle acceleration in cosmic plasmas*; edited by G. P. Zank and T. K. Gaisser, 445-450, AIP, New York, 1992.

Krauss-Varban, D., D. Burgess, and C. S. Wu, Electron acceleration at nearly perpendicular collisionless shock. 1. One-dimensional simulations without electron scale fluctuations, *J. Geophys. Res.*, *94*, 15089-15098, 1991.

Krauss-Varban, D., and D. Burgess, Electron acceleration at nearly perpendicular collisionless shocks, 2, Reflection at curved shocks, *J. Geophys. Res.*, *96*, 143-154, 1991.

Krauss-Varban, D., and C. S. Wu, Fast Fermi and gradient drift acceleration of electrons at nearly perpendicular collisionless shocks, *J. Geophys. Res.*, *94*, 15367-15372, 1989.

Krauss-Varban, D., N. Omidi, and K. B. Quest, Mode properties of low frequency waves: Kinetic theory versus Hall-MHD, *J. Geophys. Res.*, *99*, 5987-6009, 1994.

Krauss-Varban, D., F. G. E. Pantellini, and D. Burgess, Electron dynamics at quasi-perpendicular collisionless shocks, Eos *Trans. AGU, 75(44)*, Fall Meeting suppl., 529, 1994.

Lewier, P. C., V. K. Decyk, J. M. Dawson, and B. Lembege, Numerical studies of electron dynamics in oblique quasi-perpendicular collisionless shock waves, *J. Geophys. Res.*, *96*, 9455-9469, 1991.

Mellot, M. M., and E. W. Greenstadt, Plasma waves in the range of the lower hybrid frequency: ISEE 1 and 2 observations at the Earth's bow shock, *J. Geophys. Res.*, *93*, 9695-9705, 1988.

Ogilvie, K. W., J. D. Scudder, and H.Doong, The electron spectrometer experiment on ISEE 1, IEEE *Trans. Geosci. Electron.*, *16*, 261-265, 1978.

Onsager, T. G, and M. F. Thomsen, The Earth's foreshock, bow shock and magnetosheath, *U.S. Natl. Rep. Int. Union Geod. Geophys. 1987-1990, Rev. Geophys.*, *29*, 998-1007, 1991.

Orlowski, D. S., and C. T. Russell, ULF waves upstream of the Venus bow shock: Properties of one-Hertz waves, *J. Geophys., Res.*, *96*, 11,271-11,282, 1991.

Orlowski, D. S., G. K. Crawford, and C. T. Russell, Upstream waves at Mercury, Venus and Earth: Comparison of properties of one-Hertz waves, *Geophys. Res. Lett.*, *17*, 2293-2296, 1990.

Orlowski, D. S., C. T. Russell, and R. Lepping, Wave phenomena in the upstream region of Saturn, *J. Geophys. Res.*, *97*, 19187-19199, 1992.

Orlowski, D.S., C.T. Russell, D. Krauss-Varban, and N. Omidi, On the source of upstream whistlers in the Venus foreshock, in *Plasma Environments of Non-magnetic Planets* edited by T. I. Gombosi, pp. 217-227, Pergamon, New York, 1993.

Pantellini, F. G., D. Burgess, and D. Krauss-Varban, Electron thermalization at quasi-perpendicular collisionless shocks, Abstract, Eos, *Trans., AGU, 74*(43), Fall Meeting suppl., 492, 1993.

Paschmann, G., N. Sckopke, I. Papamastorakis, J. R. Asbridge, S. J. Bame, and J. T. Gosling, Beam, intermediate and diffusive proton distributions in the Earth's foreshock, *J. Geophys. Res.*, *86*, 4355-4364, 1981.

Rodriguez, P., and D. A. Gurnett, Electrostatic and electromagnetic turbulence associated with Earth's bow shock, *J. Geophys. Res.*, *80*, 19-27, 1975.

Russell, C. T., The ISEE 1 and 2 Fluxgate magnetometers, *IEEE Trans. Geosci. Electron.*, *16*, 239-242, 1978.

Russell, C. T., D. D. Childers, and P. J. Coleman, OGO 5 observations of upstream waves in the interplanetary medium, *J. Geophys.Res.*, *76*, 845-861, 1971.

Schwartz, S. J., M. F. Thomsen, W. C. Feldman, and F. T. Douglas, Electron dynamics and potential jump across slow mode shocks, *J. Geophys. Res.*, *92*, 3165-3174, 1987.

Schwartz, S. J., M. F. Thomsen, W. C. Feldman, and F. T. Douglas, Electron heating and the potential jump across fast mode shocks, *J. Geophys. Res.*, *93*, 12,923-12,934, 1988.

Scudder, J. D., A. Mangeney, C. Lacombe, C. C. Harvey, C. S. Wu, and R. R. Anderson, The resolved layer of a collisionless, high-beta supercritical, quasi-perpendicular shock wave, 3, Vlasov electrodynamics, *J. Geophys. Res.*, *91*, 11,075-11,084, 1986.

Sentman, D. D., M. F. Thomsen, S. P. Gary, W. C. Feldman, and M. M. Hoppe, The oblique whistler instability in the Earth's foreshock, *J. Geophys. Res.*, *89*, 2048-2056, 1983.

Stix, T. H., *The Theory of Plasma Waves*, McGraw-Hill, New York, 1962.

Thomsen, M. F., H. C. Barr, S. P. Gary, W. C. Feldman, and T. E. Cole, Stability of electron distributions within the Earth's bow shock, *J. Geophys. Res.*, *88*, 3035-3049, 1983.

Thomsen, M. F., J. T., Gosling, S. J. Bame, and M. M. Mellott, Ion and electron heating at collisionless shock near critical shock number, *J. Geophys. Res.*, *90*, 137-149, 1985.

Thomsen, M. F., M. M. Mellot, J. A. Stansberry, S. J. Bame, J. T. Gosling, and C. T. Russell, Strong electron heating at Earth's bow shock, *J. Geophys. Res., 92*, 10,119-10,124, 1987.

Timofeev, A.V., and V. I. Pistunovich, Rev. Plasma Physics, edited by M. A. Leontovitch, 435-449, Consultants Bureau, New York, 1970.

Tokar, R. L., and D. A. Gurnett, The propagation and growth of whistler mode waves generated by electron beams in the Earth's bow shock, *J. Geophys. Res., 90*, 105-114, 1985.

Tokar, R. L., D. A. Gurnett, and W. C. Feldman, Whistler mode turbulence generated by electron beams in Earth's bow shock, *J. Geophys. Res., 89*, 105-114, 1984.

Vaisberg, O. L., et al., Observations of lower hybrid turbulence at the Earth's shock, Rep. 813, USSR Acad. of Sci., Space Res. Institute, Moscow, 1983.

Veltri, P., and G. Zimbardo, Electron-whistler interactions at the Earth's bow shock, 1, Whistler instability, *J. Geophys. Res., 98*, 13325-13333, 1993a.

Veltri, P. and G. Zimbardo, Electron-whistler interactions at the Earth's bow shock, 2, Electron pitch angle diffusion, *J. Geophys. Res., 98*, 13,335-13,346, 1993b.

Veltri, P., A. Mangeney, and J. D. Scudder, Electron heating in quasi perpendicular shocks: A Monte Carlo simulation, *J. Geophys. Res., 95*, 14,939-14,959, 1990.

Wu, C. S., A fast Fermi process: Energetic electrons accelerated by nearly perpendicular bow shock, *J. Geophys. Res., 89*, 8857-8869, 1984.

Wong, H. K., and M. L. Goldstein, Proton beam generation of whistler waves in the Earth's foreshock, *J. Geophys.Res., 92*, 12,419-12,424, 1987.

Wong, H. K., and M. L. Goldstein, Proton beam generation of oblique whistler mode waves, *J. Geophys. Res., 93*, 4110-4114, 1988.

D. Krauss-Varban and N. Omidi, Department of Electrical and Computer Engineering and California Space Institute, University of California, San Diego, La Jolla, CA 92023-0407. (varban@ece.ucsd.edu;nomidi@ece.ucsd.edu).

D. S. Orlowski and C. T. Russell, Institute of Geophysics and Planetary Physics, University of California, 405 Hilgard Ave., 6843 Slichter Hall, Los Angeles, CA 90095-1567. (darius@igpp.ucla.edu; ctrussell@igpp.ucla.edu).

M. F. Thomsen, Los Alamos National Lab, Los Alamos, NM 87545. (mthomsen@lanl.gov).

(Received May 12, 1994; revised December 27, 1994; accepted December 29, 1994.)